Robotized Additive Manufacturing of Silicone for Skeleton-Reinforced Linear Soft Actuators

Jeremy Sand, Benoit Wach, Maciej Bednarczyk, Laurent Barbé, François Geiskopf

Robotized additive manufacturing of silicone for skeleton-reinforced linear soft actuators

Jérémy Sand[1], Benoît Wach[1], Maciej Bednarczyk[1], Laurent Barbé[1] and François Geiskopf[1] .

***Abstract*— This paper presents a method for manufacturing a soft pneumatic linear actuator. The linear actuator is based on a deformable chamber reinforced by a cylindrical auxetic structure. The objective of this work is to create a hermetic silicone chamber inside the auxetic structure previously machined in PVC. The manufacturing process is based on 3D silicone printing using an anthropomorphic robotic arm. The proposed strategy increases the versatility of the process compared to overmolding strategies, especially in regard to the dimensions of the actuator. In this paper we present an experimental setup integrating a robotic arm, the system for the registration of the different elements and the control of the print head trajectories. The actuator has been designed, built and implemented, allowing us to evaluate its performances and life span.**

I. Introduction and context

The interest in soft robotics has significantly increased in the last years. The human machine interaction is a main concern in the robotic community, seeking to provide technological solutions which are both efficient, lightweight and compliant when interacting with the environment [1]. Such properties are desired in different fields, for example in the medical field where the robot could directly be in contact with the patient and should not cause any lesions [2]. Due to their compliance with their surroundings, soft robots can answer to these needs to some extent. As shown in [3], different soft robots with functionalities such as crawling, swimming or gripping exist. They are mostly made of elastomers and actuated through cables, fluidic interaction, or electro-active polymers.

In the past, some effort was done in [4] and [5] to develop a linear actuator for medical applications taking advantage of the previously highlighted features. In their design, the authors focus on the simplest soft robot, which is a balloon that expands in all directions isotropically. A reinforcing structure is added to constraint the motion to one direction. This allows to use the rigidity of the structure to precisely guide the motion and in the same time benefit from the compliance provided by the inflatable airtight chamber. In order to achieve the desired motion, the authors designed the reinforcing structure using an auxetic skeleton, i.e. a rigid structure that exhibits a negative Poisson ratio. The auxetic skeleton transforms the radial expansion into an axial expansion, unlike a standard material, which would axially shrink. This allows to increase the achieved displacement. The principle of such a design is shown in Fig. 1, and the auxetic skeleton is based on an inverted honeycomb cell represented in Fig. 2.

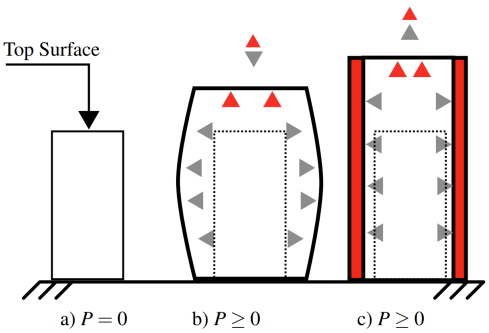

Fig. 1: Section view of the balloon: a) without pressure; b) with pressure, conventional outer envelope; c) with pressure, auxetic reinforced outer envelope. Axial and radial forces produced by internal pressure are represented by red and gray arrows respectively. [4]

Pfeil *et al.* [5] made a prototype of this actuator using multi-material additive manufacturing (MMAM). This process is used to perform 3D printing of two materials simultaneously: a soft material for the airtight chamber and a rigid material for the auxetic reinforcement. Such a process has the advantage of flexibility in design, as it allows to adapt the dimensions and thus the specifications of the structure to the needs of the desired application. However, there is a limited choice in materials available in additive manufacturing (AM) and therefore a limited range of available material properties [6]. In [4], the authors show that currently, the main limitations of the actuators manufactured using MMAM, are linked to the failure modes of the soft materials resulting in air leaks, and also their limited biocompatibility.

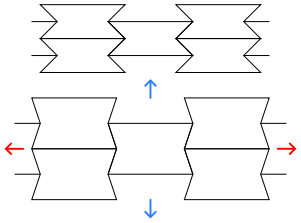

Fig. 2: Behavior of an inverted honeycomb mesh: red arrow = imposed motion; blue arrow = reaction motion

[1]ICube, UMR 7357, University of Strasbourg, CNRS, 1 place de l'Hopital, 67091, Strasbourg, France. Corresponding author: j.sand@unistra.fr This paper has supplementary downloadable material available at http://ieeexplore.ieee.org, provided by the authors. This includes a multimedia mp4 format movie clip, which shows the manufacturing process. This material is 16.5 MB in size

In order to overcome these limitations, another manufacturing process for creating soft robots of centimetric scale is molding or injection molding [7]. These processes can be used to manufacture bio-compatible materials, such as silicone, with higher elongation at break, improving the durability of the actuator. However, it comes with an increase of manufacturing time and costs resulting from the need of creating a dedicated mold for each desired dimensions [8].

In this work, we aim at providing a new manufacturing process in order to combine the advantages of silicone molding and 3D printing. The recent progress in silicone AM showed that it is possible to manufacture silicone volumes without a mold [9], and that it can also be used for the manufacturing of pneumatic actuated soft robots as demonstrated in [10]. In our approach, we propose to use silicone AM to manufacture a silicone chamber inside a machined auxetic skeleton, while avoiding collisions between the skeleton and the silicone printhead. By considering the axisymmetric nature of the silicone filament, the robotic 3D printing task requires five degrees of freedom (DoF). In [11], the authors demonstrated the use of a robot for AM purposes. To the best of our knowledge, the AM of silicone with a robotic arm has not yet been done in the literature.

The rest of this paper is structured as follows: In section II the design of the linear actuator and the manufacturing process are introduced. Then, in section III and IV the manufacturing process and the actuator performances are evaluated. Finally, in section V, conclusion on the manufactured actuator and the new process and further perspectives are discussed.

II. Design of the Manufacturing Process

The proposed robotized additive manufacturing of silicone (RAMoS) device, is composed of three sub-systems: a 6 DoF anthropomorphic robotic arm, a printing bed with a positioning element for the auxetic structure and a printhead for silicone (Fig. 3). In this work, the KUKA LBR-IIWA 14 robotic arm is used. It is a seven axes anthropomorphic robotic arm, which due to its redundancy allows for a higher flexibility in positioning and obstacle avoidance. The print material is an RTV monocomponent silicone (Neutral silicone A8 Pro, Wurth), i.e. it cures at room temperature catalyzed by the ambient humidity. The silicone is extruded with the viproHead-5 from Viscotec.

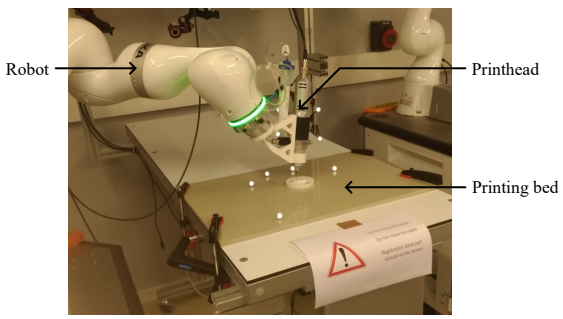

Fig. 3: Photo of the RAMoS setup

In the following section, the adaptations of actuator design, the workflow of the printing process, the registration steps, trajectory planning and printing parameters are presented.

A. Adaptation of the actuator design

The proposed product is a linear actuator with a rigid auxetic skeleton closed on the top and bottom with rigid lids and airtight thanks to an hermetic silicone chamber. The manufacturing of the silicone chamber of the actuator with RAMoS requires some adaptations of the actuators design. Indeed, the manufacturing of the chamber should take into account the mechanical properties of silicone and the printing nozzle should go inside the auxetic cylinder to deposit the silicone on the walls without any collisions.

Due to the viscous state of silicone during the printing process, we first exclude the possibility of using bridging to close the silicone chamber on the top. However, the silicone is viscous enough to stick on a surface even against the action of gravity. The proposed solution uses that property to print a first part of the silicone chamber on the auxetic skeleton and a second part on the closing lid, as represented on Fig. 4. The silicone volumes are made to overlap and are assembled before they harden on the surface (15 min with the used silicone). This allows them to fuse together and create an airtight chamber after curing. Furthermore, the hole introduced in the chamber for the air supply can introduce an air leak. Indeed, under the pressure, the silicone can warp away from the walls. To prevent this, an insert and nut are added to the air supply hole, which will compress the silicone unto the lid to create a gasket and prevent warping.

To avoid collision between the printhead and the auxetic skeleton, the printhead needs to be tilted during the printing process. However, due to its bulkiness, there are dimensions, especially in height, for which it is not possible to avoid collisions between both parts, as represented on Fig. 5. To lift the height constraint, an assembly of multiple auxetic skeletons is proposed. The assembly is designed such as all geometries can be milled. The positioning is achieved through a centering of both cylinder and a vee hollowed in complementary shapes on both auxetic skeletons. The clamping of both parts is achieved through a bayonet mount with a clipping feature, as shown in Fig. 6. The assembly could be performed on the collar, but it would reduce the

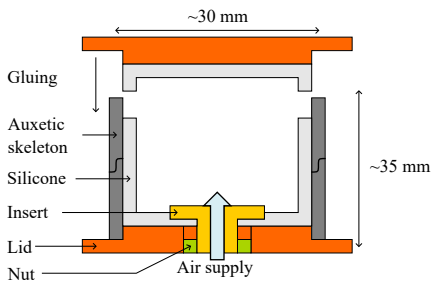

Fig. 4: Section of the linear actuator design: orange = lids; dark gray = auxetic skeletons; light gray = silicone; yellow = insert; green = nut

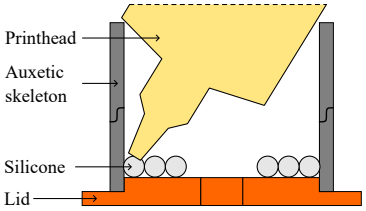

Fig. 5: Printhead positioned in the auxetic skeleton: orange = lids; dark gray = auxetic skeletons; light gray = silicone; yellow = printhead

overall performances because the collar does not exhibit auxetic properties. Instead, the assembly is realized on the rhombus which is the link between the auxetic meshes, therefore it does not contribute to the auxetic behavior and is theoretically under a null stress [12].

B. Printing process workflow

The printing process workflow can be seen in Fig. 7. The process starts with the setup steps. Then they are multiple printing steps intersected with manipulations on the actuator. The auxetic skeleton is milled in PVC, which has a high elongation at break (>40%). To assemble the lid on the auxetic skeleton, a bicomponent cyanoacrylate glue is used (Loctite 3090, Henkel).

C. Registration

Unlike traditional cartesian 3D printers, all the subsystems are not rigidly linked to each other and a bed leveling system is not included. The printhead (frame $\mathcal{B}_h$) is positioned on the robot flange (frame $\mathcal{B}_f$) with a mechanical interface of known dimensions. The robot is positioned on a base (frame $\mathcal{B}_0$) unlinked to the printing bed (frame $\mathcal{B}_b$), and the auxetic skeleton (frame $\mathcal{B}_a$) is mechanically positioned on the printing bed. However, for each printing, a nozzle (frame $\mathcal{B}_n$) is mounted on the printhead with varying depth. This depth is measured with a caliper. The previous frames are represented on Fig. 8. Through the kinematic model (KM) of the robot, the mechanical positioning, the nozzle size and the caliper measure the transform between each frame are known, except for the one between the robot base and the printing bed.

To determine the transform between $\mathcal{B}_b$ and $\mathcal{B}_0$, three markers are added to the printing bed to perform a registration. The positions of these markers are known in $\mathcal{B}_b$. With a custom-made rigid nozzle and the KM of the robot, the positions of the markers are computed in $\mathcal{B}_0$ by positioning

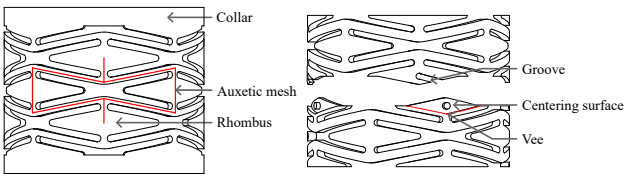

Fig. 6: CAD of an auxetic skeleton (left) and its assembly mechanism (right)

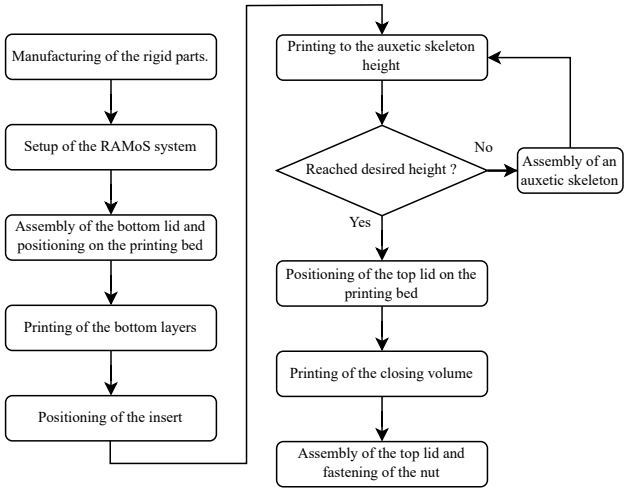

Fig. 7: Printing process workflow

the nozzle on the markers. Finally, the transform is computed using the Horn method [13].

D. Trajectory planning

The middleware ROS2 [14] is used for the planning and control of the robot and the silicone extrusion. The trajectory planning of the robot is checked with a simulation. To do so, the IIWA14 package [15] is used with the MoveIt2 package [16]. The first one implements configuration, simulation and control for the LBR-IIWA14 robot, while the second one provides a wide range of trajectory planing algorithm for robots. The used planning algorithm is the PILZ industrial planner which is used to generate linear (LIN) and circular (CIRC) motions. To plan the trajectories, a trapezoidal velocity profile is generated from a given max acceleration γ and max speed v. Points are then sampled from this profile at a given time step Δt. Finally, they are converted to joint values with the robot inverse KM. Motion blending can also be used, and allows a motion to start while the previous one is not yet finished. This is particularly useful if we want to prevent the robot from stopping between each motion. For a blending between two motions, when the motions enter a given blend radius r_b from the transition point, both motions are interpolated together by a weighted mean, where the weight is the minimum jerk path generation equation [17].

E. Slicing

To determine the trajectory and extrusion data, a slicing step adapted from [9] is applied on the silicone volume. The silicone cord section is assumed elliptical, which after deformation fills a rectangle with dimension $\Delta_w \times \Delta_h$. Therefore, the silicone volume is first cut in discs of height Δ_w, then each disc is cut in unconnected concentric circles spaced of $\alpha\Delta_h$, α being an overlap percentage. With the results of the previous step, the cartesian path of the nozzle tip can be fully defined. Moreover, an orientation is chosen which complies with the non-collision constraint. From its vertical position, the nozzle is tilted inwards from a tilt angle ϕ around the tangent of its current position on the cartesian

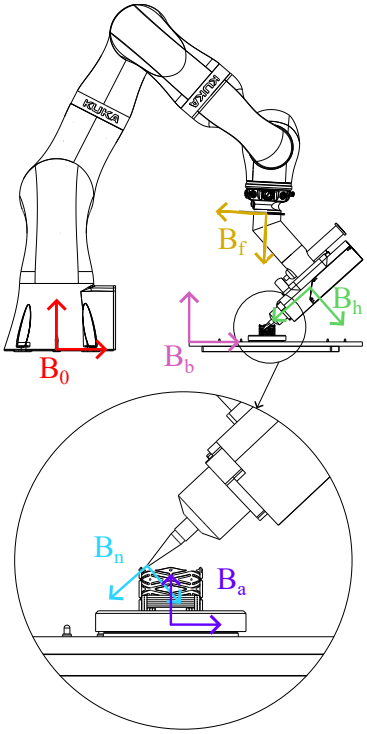

Fig. 8: Frames of the hardware setup: $\mathcal{B}_0$ = base frame; $\mathcal{B}_f$ = robot flange frame; $\mathcal{B}_h$ = printhead frame; $\mathcal{B}_n$ = nozzle frame; $\mathcal{B}_a$ = auxetic skeleton frame; $\mathcal{B}_b$ = printing bed frame

path, as represented on Fig. 9. Due to an axial symmetry of the printing nozzle, the defined path has only five DoF. Therefore, the x-axis of the nozzle is defined to be parallel to the vector linking the robot base to the auxetic skeleton center. Finally, a trapezoidal velocity profile is added to the defined six DoF path, thus each circle is realized with a CIRC motion. The acceleration phases of the trajectory are assumed to be negligible in front of the constant speed phases, therefore the silicone flow rate can be computed by $Q_s = \Delta_w \Delta_h v$, with v the max nozzle speed.

In order to achieve a smooth silicon cord, it is important to print it with a constant velocity on the entire layer. To achieve this, each layer will be realized with one silicone cord. To transition between each circle at a constant speed, two successive CIRC motion are blended together with an

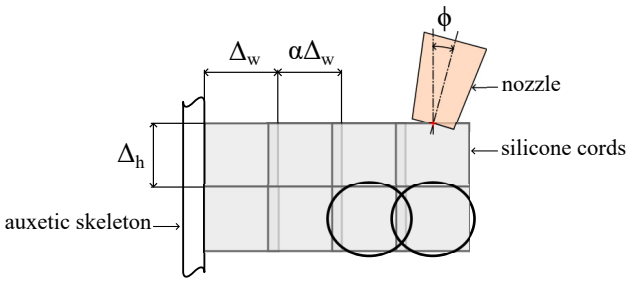

Fig. 9: Sliced silicone cords and tilted nozzle pose: Δ_h = layer height; Δ_w = layer width; α = overlap percentage; ϕ = tilt angle

intermediary LIN motion. The result of such a blending can be seen in Fig 10. The arc length L_a defines the distance of transition between two circles. PILZ does not allow two blend radii to overlap, therefore there is a minimum value for L_a. Using the law of cosine, and noting R_1 and R_2 the radius of the outer and inner circle respectively, and ε the planner precision, we can compute $L_{a,min}$ as noted in equation (1).

$$L_{a,min} = R_1 \cos^{-1}\left(\frac{R_1^2 + R_2^2 - (2r_b + \varepsilon)^2}{2R_1R_2}\right) \quad (1)$$

The blend radius is chosen such as the mean velocity is maintained. Considering that each velocity profile has the same acceleration γ and velocity v, mean velocity is maintained if the blending is performed during the acceleration/deceleration phases. Therefore, the blending radius is equal to the distance traveled during one acceleration phase, as expressed in equation (2).

$$r_b = \frac{v^2}{2\gamma} \quad (2)$$

During the transition between the circles, the orientation of the nozzle is defined as a quaternion slerp [18] between the orientations at the end of the outer CIRC motion (R_1 radius) and at the beginning of the inner CIRC motion (R_2 radius).

III. Evaluation of the Manufacturing Process

A. Single part auxetic skeleton actuator

To demonstrate the manufacturing process, multiple actuators were manufactured with it. Two actuators with a single part auxetic skeleton were manufactured, meaning that no assembled auxetic skeleton were involved in these designs. The auxetic skeletons have a dimension of ∅30.4 mm x 23.9 mm and have four radial and two axial auxetic meshes. Because the main concern of our work is airtightness, and not geometrical accuracy, a ∅1.6 mm nozzle is used, thus to match that diameter, the cords dimensions are $\Delta_h = \Delta_w = 1.6$ mm and $\alpha = 1.0$. For security reason linked to the use of a robot, a low velocity of $v = 3$ mm/s is chosen. Given that a cord is 1.6 mm wide, we expect the start and end point of a circle to connect if $L_a \leqslant 1.6$ mm. Such a value is reachable without a software error in planing step for $r_b = 0.8$ mm, therefore $\gamma = 5.6$ mm/s^2. The tilt angle used was of $\phi = 10°$ for which collisions are avoided. Finally, to achieve airtightness, an

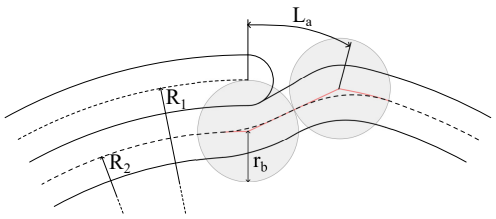

Fig. 10: Transition trajectories between two circles of a disc with the extruded cord: dashed line = nozzle path; red line = pre-blending path; gray circles = blending circles; L_a = arc length; R_1 = outer CIRC motion radius; R_2 =inner CIRC motion radius; r_b = blending radius

Fig. 11: Slice of a silicone print with $\phi = 10°$ with the nozzle axis: z axis of the nozzle

overlap of the silicone volumes of 1.6 mm is also introduced. To achieve the printing process, the registration step has been performed once, and the setup maintained fixed between each print.

The main difference between the actuators is the thickness of the silicone walls. The first actuator (Actuator 1) was done with a thickness of 3.2 mm, meaning two silicone cords of thickness. While the second actuator (Actuator 2) was done with a thickness of 1.6 mm, meaning one silicone cord of thickness. A slice of a print achieved with two silicone cords can be seen on figure 11. To verify their airtightness, a 100 kPa input was applied to the actuator. Actuator 1 proved to be airtight, while Actuator 2 had air leaks. We can expect that increasing the number of silicone cords per wall, increasing the overlap of the silicone volumes, or decreasing α, will positively impact the airtightness. Therefore, the geometric parameters of the silicone chamber from Actuator 1 would be the minimum values to achieve an airtight part with RAMoS and a ∅1.6 mm nozzle.

B. Assembled auxetic skeleton actuator

Using the same parameters as for Actuator 1 an actuator with an assembly of two auxetic skeletons was manufactured. In this case, the auxetic skeletons have a dimension of ∅33.7 mm x 47.2 mm and have four radial and two axial auxetic meshes each. Furthermore, these skeletons were not machined in PVC because the milling of the designed bayonet mounts was not studied yet. Instead, they are manufactured in a photopolymer (Vero STRATASYS) thanks to polyjet AM (STRATASYS J826).

An actuation of 100 kPa showed that this actuator was also airtight. However, under the deformation due to the actuation, the bayonet mounts broke. This failure can be linked to the use of Vero and polyjet AM, which we know is more fragile than milled PVC.

IV. Evaluation of the actuator performances

A. Experimental protocol

The Actuator 1's performances have been tested in displacement and life span. In order to control the actuator during these tests, a pneumatic distribution bench was designed. It is composed of a proportional valve (VPPM series, Festo) for the pressure regulation and a fast 3/2-way solenoid valve (MHE2 series, Festo) to trigger the output. The air pressure delivered is measured with a pressure sensor (SPTW series, Festo). A custom software running under a real-time operating system (Linux Xenomai) is used to synchronize all sensor acquisitions with the control of the distribution at a sampling rate of 1kHz. A fast sampling rate telemeter (Microepsilon OptoNCDT 2420) is used to acquire the displacement of the actuator. A break-in test is performed on the actuator. More than 150 cycles are achieved with a 0.5 Hz, 50% duty cycle, 100kPa square wave.

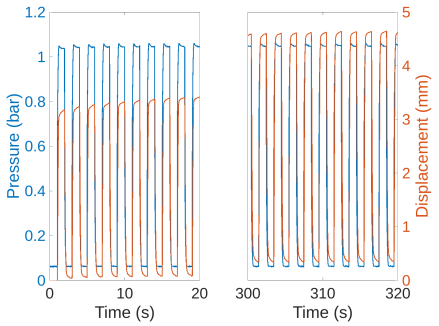

Fig. 12: Start and end of the break-in test of Actuator 1 (steady increase in between)

B. Results

During the break-in test, no signs of wear, were visible on the auxetic skeleton or the silicone chamber. As we can see on Fig. 12, the maximum displacement of the actuator showed a steady increase during the break-in. The displacement at the start of the break-in is of 3.2 mm and the displacement at the end of the break-in is of 4.3 mm, which is an increase of performances of 34%. Relative to the length of the auxetic skeleton, we have a respective deformation of 13.4% and 18.0%. However, as we can see on Fig. 13, the motion is not straight. This is a decrease in performance compared to the designs presented in [4] or [5] which are manufactured in MMAM.

V. Discussion and conclusion

In this paper, a robotized additive manufacturing of silicone process dedicated to a pneumatic soft actuator with auxetic reinforcement has been proposed. The additive manufacturing environment has been developed and some adaptations of the actuators structure have been made in order to meet the constraints of RAMoS. We hereby give the first proof of concept, to our knowledge, of the use of RAMoS

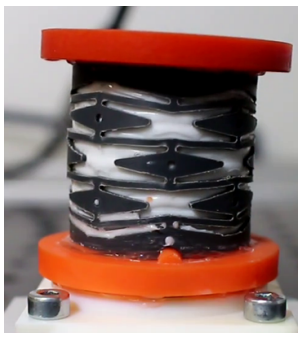

Fig. 13: Actuated Actuator 1

for the manufacturing of an airtight silicone chamber on a rigid structure. The results showed that in order to achieve air-tightness, at least two silicone cords are required on the walls. Indeed, the second circle printed in continuity with the first one closes the gap between the start and end of the first circle.

The manufactured actuator can be compared to the design of similar dimension (∅27 mm x 25 mm) presented in [4] and manufactured with MMAM. This design presented by Schmitt *et al.* is easily subject to material failure. Unlike the Actuator 1 manufactured with RAMoS which is shown to be durable. Therefore, RAMoS is shown to be a manufacturing process for soft robots which keeps the flexibility of AM while producing parts with a notable increase in durability compared to the MMAM design. Furthermore, the actuator manufactured with MMAM showed a relative displacement of $\varepsilon = 10.7\%$, while the Actuator 1 could reach a relative displacement of $\varepsilon = 18.0\%$. This displacement was reached with a lower pressure (250kPa and 100kPa respectively), which is linked to the use of softer material in our design. However, in our design the motion is warped, which is a loss in performance compared to the other design and requires improvement.

A study of the functional actuators showed two possible sources for the warped motion. We noticed that the direction of warping is the same as the position of the transition between the printed circles. This transition introduces a lack of silicone in one direction, which might explain the warping through an heterogeneity of the print along the radius. Otherwise, it can also be linked to the registration between the robot base and the auxetic skeleton. The fixed setup means that any registration error which introduces a centering error between the auxetic skeleton and the silicone volume would be present on each part. As previously, the centering error can induce an heterogeneity along the radius and therefore a warped motion.

These problems could be solved by improving RAMoS. A synchronization between the robot and the extruding system, and an implementation of the extrusion control which take into account the acceleration phases of the robot and printhead could be introduced. A new trajectory could then be proposed, which is homogenous along the radius. A registration method which is more precise can also be implemented and the automation of some steps of the manufacturing process can be considered.

Further development can be conducted on the assembly of auxetic skeletons. A study of the machining of a bayonet mount should be conducted to determine if the failure was due to the material used or the design in itself, and in the second case, a new assembly process can be proposed.

Fig. 11 also highlight a tilt in the silicone cords which is not present in cartesian printing [9]. A study of these results can be conducted to propose a new model for the silicone cords and a slicing strategy adapted for 5 axis silicone AM.

ACKNOWLEDGMENT

The authors would like to thank Loïc Mosser for his knowledge and assistance in silicone AM. This work of the Interdisciplinary Thematic Institute HealthTech, as part of the ITI 2021-2028 program of the University of Strasbourg, CNRS and Inserm, was supported by IdEx Unistra (ANR-10-IDEX-0002) and SFRI (STRAT'US project, ANR-20-SFRI-0012) under the framework of the French Investments for the Future Program. This work has been partially supported by ROBOTEX 2.0 (Grants ROBOTEX ANR-10-EQPX-44-01 and TIRREX ANR-21-ESRE-0015), Labex CAMI (ANR-11-LABX-0004) funded by the French program Investissements d'avenir.

REFERENCES

[1] S. Kim, C. Laschi, and B. Trimmer, "Soft robotics: a bioinspired evolution in robotics," Trends in biotechnology, vol. 31, no. 5, pp. 287–294, 2013.

[2] M. Runciman, A. Darzi, and G. P. Mylonas, "Soft robotics in minimally invasive surgery," Soft robotics, vol. 6, no. 4, pp. 423–443, 2019.

[3] C. Lee, M. Kim, Y. J. Kim, N. Hong, S. Ryu, H. J. Kim, and S. Kim, "Soft robot review," International Journal of Control, Automation and Systems, vol. 15, no. 1, pp. 3–15, 2017.

[4] F. Schmitt, O. Piccin, B. Bayle, P. Renaud, and L. Barbé, "Inverted honeycomb cell as a reinforcement structure for building soft pneumatic linear actuators," Journal of Mechanisms and Robotics, vol. 13, no. 1, 2021.

[5] A. Pfeil, L. Barbe, B. Wach, A. Bruyas, F. Geiskopf, M. Nierenberger, and P. Renaud, "A 3d-printed needle driver based on auxetic structure and inchworm kinematics," in International Design Engineering Technical Conferences and Computers and Information in Engineering Conference, vol. 51807. American Society of Mechanical Engineers, 2018, p. V05AT07A057.

[6] S. Singh, S. Ramakrishna, and R. Singh, "Material issues in additive manufacturing: A review," Journal of Manufacturing Processes, vol. 25, pp. 185–200, 2017.

[7] F. Schmitt, O. Piccin, L. Barbé, and B. Bayle, "Soft robots manufacturing: A review," Frontiers in Robotics and AI, vol. 5, p. 84, 2018.

[8] M. Bont, C. Barry, and S. Johnston, "A review of liquid silicone rubber injection molding: Process variables and process modeling," Polymer Engineering & Science, vol. 61, no. 2, pp. 331–347, 2021.

[9] J. Plott and A. Shih, "The extrusion-based additive manufacturing of moisture-cured silicone elastomer with minimal void for pneumatic actuators," Additive Manufacturing, vol. 17, pp. 1–14, 2017.

[10] F. Weigand, A. M. Nguyen, J. Wolff, and A. Seibel, "Toward industrial silicone 3d printing of soft robots," in 2021 IEEE 4th International Conference on Soft Robotics (RoboSoft). IEEE, 2021, pp. 523–526.

[11] L. D. Evjemo, S. Moe, J. T. Gravdahl, O. Roulet-Dubonnet, L. T. Gellein, et al., "Additive manufacturing by robot manipulator: An overview of the state-of-the-art and proof-of-concept results," in 2017 22nd IEEE International Conference on Emerging Technologies and Factory Automation (ETFA). IEEE, 2017, pp. 1–8.

[12] L. J. Gibson, M. F. Ashby, G. Schajer, and C. Robertson, "The mechanics of two-dimensional cellular materials," Proceedings of the Royal Society of London. A. Mathematical and Physical Sciences, vol. 382, no. 1782, pp. 25–42, 1982.

[13] B. K. Horn, H. M. Hilden, and S. Negahdaripour, "Closed-form solution of absolute orientation using orthonormal matrices," JOSA A, vol. 5, no. 7, pp. 1127–1135, 1988.

[14] Y. Maruyama, S. Kato, and T. Azumi, "Exploring the performance of ros2," in Proceedings of the 13th International Conference on Embedded Software, ser. EMSOFT '16. New York, NY, USA: Association for Computing Machinery, 2016. [Online]. Available: https://doi.org/10.1145/2968478.2968502

[15] "Iiwa ros2. github," https://github.com/ICube-Robotics/iiwa_ros2/tree/main, accessed Sept. 30, 2022.

[16] "Moveit. github," https://github.com/ros-planning/moveit2, accessed Oct. 14, 2022.

[17] K. Kyriakopoulos and G. Saridis, "Minimum jerk path generation," in Proceedings. 1988 IEEE International Conference on Robotics and Automation, 1988, pp. 364–369 vol.1.

[18] J.-s. Ahn, W.-j. Chung, and C.-d. Jung, "Realization of orientation interpolation of 6-axis articulated robot using quaternion," Journal of Central South University, vol. 19, no. 12, pp. 3407–3414, 2012.